An energetically consistent vertical mixing parameterization in CCSM4

Søren B. Nielsen[a,*], Markus Jochum[a], Carsten Eden[b], Roman Nuterman[a]

[a] *Climate and Computational Geophysics, Niels Bohr Institute, University of Copenhagen, Copenhagen, Denmark*
[b] *Institut für Meereskunde, University of Hamburg*

Abstract

An energetically consistent stratification-dependent vertical mixing parameterization is implemented in the Community Climate System Model 4 and forced with energy conversion from the barotropic tides to internal waves. The structures of the resulting dissipation and diffusivity fields are compared to observations, and the fidelity of the resulting temperature fields is assessed. Compared to existing biases in the control simulation, differences in surface fields are small, showing that the surface climate state is relatively robust to the choice of mixing parameterization. The thermocline structure, however, depends greatly on the details of the vertical mixing parameterizations, where the new energetically consistent parameterization results in low thermocline diffusivities and a sharper and shallower thermocline. It is also investigated if the ocean state is more sensitive to a change in forcing if the energetically consistent scheme is used compared to a tidal mixing parameterization with fixed background diffusivity. In particular we find that the Atlantic Meridional Overturning Circulation is more sensitive to changes in the Southern Ocean wind stress with the former. However, in line with previous results, changes to Southern Ocean upwelling are still largely compensated by changes to the diabatic upwelling in the Indo-Pacific basin.

Keywords: Diapycnal mixing, Numerical mixing, Parameterizations, Internal wave breaking

1. Introduction

Mechanical energy is needed to return the deep waters that are formed at high latitudes to the surface (see e.g. Sandström, 1908). It has been

*Corresponding author: Juliane Maries Vej 30, 2100 Copenhagen, Denmark
Email address: soeren.nielsen@nbi.ku.dk (Søren B. Nielsen)

Preprint submitted to Ocean Modelling *March 21, 2018*

hypothesized that this mechanical energy is provided by the breaking of internal waves to small scale turbulence (Munk, 1966; Munk and Wunsch, 1998). This hypothesis has been supported by numerical studies (Bryan, 1987; Marotzke, 1997). Yet, despite its importance, small scale turbulence in the ocean interior is still represented through diffusivity, fixed in time and space. More recently, this so called background diffusivity will be amplified near the bottom to mimic tidally induced mixing (e.g. Bryan and Lewis, 1979; St. Laurent et al., 2002). However, for large parts of the ocean, away from the boundary layers, the vertical diffusivity is dominated by the background diffusivity.

The value of this background diffusivity is obtained by a combination of observations and model optimization. Using spatially-varying maps of diffusivity to match global observations rather than a constant global value has been shown to improve climate models (Harrison and Hallberg, 2008; Jochum, 2009). However, while using a constant diffusivity can yield pre-industrial or present day simulations in good agreement with observations, the reliability of these parameterizations is questionable for different climate states. The model of Osborn (1980) suggests that vertical diffusivity, κ, is a function of locally dissipated energy from the internal wave field, ϵ, and the Brunt-Väisälä frequency, N,

$$\kappa \propto \frac{\epsilon}{N^2}. \tag{1}$$

Because both variables are likely to change as climate changes, we expect changes in diffusivities and therefore in ocean circulation, heat and carbon storage and uptake. Furthermore, present tidal mixing parameterizations have problems of representing observed dissipation rates due to assumptions regarding the propagation and dissipation of internal wave energy (Waterhouse et al., 2014; MacKinnon et al., 2017; Kunze, 2017).

The focus of this study is how climate is affected when using an energetically consistent mixing parameterization rather than using fixed background diffusivities. Studies suggest that the parameterization of interior mixing affects the simulations of pre-industrial climate (e.g. Jayne, 2009; Melet et al., 2013). In particular, changes in the localization of dissipation of internal wave energy has consequences in regions of deep water formation as well as for thermocline structure (Melet et al., 2013, 2016). Previous studies mainly focus on steady state properties of the ocean; here we perform a simple experiment to assess to what degree the ocean response to changed forcing is affected by the choice of parameterization.

The topic of interest for this experiment is the strength of the Atlantic Meridional Overturning Circulation (AMOC). The AMOC is a measure of the volume transport from the Southern Hemisphere to the Northern, often referred to as the "ocean conveyor belt", with sinking waters in the North Atlantic being replaced by sub-tropical surface waters through the Gulf Stream. This circulation gives rise to an Atlantic heat transport from the Southern to the Northern hemisphere. The driving mechanisms of the AMOC have been investigated and discussed throughout the last decades (see e.g. the review by Kuhlbrodt et al., 2007). In particular, buoyancy fluxes, diapycnal mixing rates and Southern Ocean wind stress have all been suggested to play important or even dominating roles. These also impact the strength of the Antarctic Circumpolar Current (ACC) (Gent et al., 2001). Several numerical studies have implicated a direct dependency of overturning to the value of diapycnal diffusivity (Bryan, 1987; Marotzke, 1997). Yet, many studies require mixing values larger than observed to sustain the observed rate of overturning (Toggweiler and Samuels, 1995; Polzin et al., 1997; Ledwell et al., 1998).

In the mid 1990's it was pointed out that Southern Ocean winds and the sill at the Drake Passage were potentially dominating global ocean upwelling, sometimes referred to as the "Drake Passage Effect" (Toggweiler and Samuels, 1995). Even near the limit of no vertical diffusion, the Drake Passage Effect was discovered to sustain an observed overturning (Toggweiler and Samuels, 1998). In a more recent study, Munday et al. (2013) found the overturning to be less sensitive to wind forcing as horizontal resolution increased due to the explicit generation of Southern Ocean eddies, although a sensitivity remained. Additionally, the overturning was found to be sensitive to the choice of diapycnal diffusivity regardless of model resolution. All these results were obtained by forcing an ocean model with prescribed buoyancy forcing.

In contrast to these studies Jochum and Eden (2015) found that in a realistic coupled climate model the AMOC is robust to changes in Southern Ocean wind stress: Changes to Southern Ocean winds and upwelling are compensated by diabatic upwelling in the Indo-Pacific basin. Their study, however, used a fixed vertical diffusivity, so that changed mixing rates due to changed ocean stratification are not present, possibly leading to an overestimation of the Indo-Pacific compensation. Here we will revisit this idea and check if their results still hold if a fixed-energy, rather than a fixed-diffusivity parameterization is used.

The paper is structured as follows: In section 2 current ideas about di-

apycnal mixing and its parameterizations are briefly reviewed, and an energetically consistent parameterization (IDEMIX, Olbers and Eden, 2013) and its implementation in an ocean model are described. In Section 3 the results of model simulations with the standard mixing parameterization and with IDEMIX are compared in two sets: three coupled simulations (including a sensitivity study), and six forced simulations, comparing the response of the ocean to changes in the wind stress under the two different mixing schemes. In Section 4 the results are summarized and discussed in context to modelling, climate and future prospects.

2. Methods

2.1. Vertical mixing in ocean models

Diapycnal (from hereon simply vertical) mixing in the ocean in level coordinate ocean general circulation models is generally represented as a vertical diffusion of tracers. This process represents the conversion of small scale turbulent kinetic energy into potential energy and is important in setting the global pycnocline structure (Munk, 1966). It is often recognized that an average global value of 10^{-4} m^2s^{-1} is required to maintain the observed global stratification (Munk and Wunsch, 1998).

The energy input needed to maintain the observed ocean stratification has been estimated to be approximately 2 terawatts (TW), partitioned between winds and tides (Munk and Wunsch, 1998; Egbert and Ray, 2000; Jayne and St. Laurent, 2001; Nycander, 2005). Wind energy enters the ocean through the work winds do on the surface ocean, with a large fraction driving the time-mean circulation, eventually dissipating to mesoscale eddies, and some through direct generation of near-inertial waves (NIWs, see e.g. Jochum et al., 2013), of which only a fraction leaves the mixed-layer. Energy from mesoscale eddies is lost through numerous processes, including bottom and lateral friction and generation of lee waves over rough topography in a similar way as tidal energy loss (Nikurashin and Ferrari, 2010). Estimates of dissipation and diffusivity from Argo float finestructure measurements support the relationship between vertical mixing and dissipation of barotropic tides as well as geostrophic motions (Whalen et al., 2012; Pollmann et al., 2017).

With the recognition of the importance of tides and their signature bottom enhanced mixing, parameterizations have been developed for tidally induced mixing near the bottom. One such parameterization is the one by

St. Laurent et al. (2002). This parameterization calculates a bottom enhanced diffusivity based on the local energy flux from tides to internal waves (taken from the model of tidal dissipation by Jayne and St. Laurent, 2001), by assuming that a fraction, q, of the energy that is locally converted from barotropic to internal tides is dissipated locally through a vertical distribution function which ensures bottom enhanced mixing, whereas the remaining energy radiates away and contributes to background mixing (for details, see Simmons et al., 2004; Jayne, 2009). The mathematical expression becomes

$$\kappa = \kappa_b + \frac{q\Gamma E_{F,t}(x,y)F(z)}{\rho N^2}, \tag{2}$$

where κ_b is the background diffusivity, $\Gamma = 0.2$ is the mixing efficiency and $q = 1/3$ is the fraction of the energy flux from barotropic tides to internal waves, $E_{F,t}$, that dissipates locally, with the local dissipation being distributed vertically by an exponential decay function, $F(z)$ and ρ being the density.

One key uncertainty is the fixed vertical decay scale, $F(z)$, for the dissipation of internal wave energy. This choice often does not match observations (Kunze, 2017), and it has been shown that the choice of a vertical dissipation profile is important for setting the ocean state (Melet et al., 2013). Furthermore, the globally constant value of locally dissipated energy in Eq. 2, q, relies on sparse observations and there is little justification that one value is representative of the entire ocean (Waterhouse et al., 2014). Recent work has now provided a theoretical background to take a step in parameterizing small scale turbulence through directly computed values for dissipated energy, as described below.

2.2. IDEMIX

A recent paper proposes the model Internal Wave Dissipation, Energy and Mixing (IDEMIX, Olbers and Eden, 2013), to be implemented in a global ocean model. Although extensions to the model have been developed (Eden and Olbers, 2014), we will here use the first version as described in Olbers and Eden (2013) due to the simplicity and as the main focus is how the ocean and climate responds when the vertical mixing is defined from a constant energy flux compared to a fixed background diffusivity in space and time.

Through a set of assumptions and simplifications, IDEMIX calculates the total internal wave energy, E, as well as the dissipation of internal wave

energy, ϵ_{IW}. E is calculated by solving a single differential equation obtained from the spectral radiation balance of a weakly interacting wave field:

$$\frac{\partial E}{\partial t} - \frac{\partial}{\partial z}\left(c_0 \tau_v \frac{\partial c_0 E}{\partial z}\right) - \nabla_h \cdot v_0 \tau_h \nabla_h v_0 E = -\epsilon_{IW} + \mathcal{S}, \tag{3}$$

where the second and third terms on the l.h.s. are the vertical and horizontal transport of E, respectively. $\mathcal{S}$ represents the sum of local sources of internal wave energy.

IDEMIX has been discussed in several papers already, (Olbers and Eden, 2013; Eden et al., 2014; Eden and Olbers, 2014; Pollmann et al., 2017) and will therefore only be summarized briefly here. In order to arrive at Eq. 3, upward and downward propagating waves are first treated separately, and the wave energy is integrated over all wave numbers in each vertical wave number half-space. Equations for the sum of energy, E, and difference, ΔE, of the two half-spaces are then simplified by assuming approximate symmetry in vertical wave number, m, and that nonlinear wave-wave interactions work to eliminate ΔE through an exponential relaxation with decay scale τ_v. The wave speed is also assumed to have the same value for the upward and downward propagating waves, c_0. The value of c_0 can be found by assuming a Garrett-Munk (GM) like internal wave energy spectrum. The third term on the l.h.s. of Eq. 3 represents the lateral propagation of energy, with v_0 a horizontal average group velocity and τ_h a relaxation time for horizontal anisotropies (similar to τ_v).

The model is closed on the r.h.s. of Eq. 3 by setting

$$\epsilon_{IW} = \mu_0 f_e \frac{m_\star^2}{N^2} E^2, \tag{4}$$

which represents the energy flux at high vertical wavenumber (a combination of calculations of McComas and Müller, 1981; Heyney et al., 1986) with $m_\star$ the bandwidth in vertical wavenumber and μ_0 a constant (McComas and Müller, 1981). Finally, $f_e = f \operatorname{arccosh}(N/f)$.

The dissipation of energy is then related to a vertical diffusivity through the Osborn (1980) model:

$$\kappa = \frac{\delta}{1+\delta}\frac{\epsilon_{IW}}{N^2} = \frac{\delta}{1+\delta}\mu_0 f_e \frac{E^2}{c_\star^2 N^2}, \tag{5}$$

where the relation $m_\star = N/c_\star$ is used with $c_\star = \frac{1}{j_\star \pi}\int_{-h}^{0} N(z)dz$, with $j_\star$ the modal bandwidth of the GM-model.

2.3. Model and Implementation

Eq. 3 is implemented in the ocean component of the Community Climate System Model 4 (CCSM4, Gent et al., 2011), the Parallel Ocean Program (POP2, Danabasoglu et al., 2012) following the implementation of Eden et al. (2014) with the parameter values suggested by Olbers and Eden (2013): $\mu_0 = 4/3$, $\delta = 0.2$, $j_\star = 10$, $\tau_v = 1$ day and $\tau_h = 10$ days. First, Eq. 3 is solved with a tri-diagonal solver without the lateral propagation term, which is then added explicitly to the solution afterwards. Diffusivities obtained through Eq. 5 are capped at a minimum of 10^{-7} m^{2}s^{-1} (molecular level) and a maximum of 10^{-2} m^{2}s^{-1}.

A total of 9 experiments are carried out using the coarse resolution version of CCSM4 (Shields et al., 2012). The ocean component uses a horizontal nominal 3° resolution with 60 vertical layers of increasing thickness. In the surface layers are 10 m thick, ranging to several hundred meters in the deepest ocean. First, a coupled control simulation using the T31 × 3 configuration, CONT, is run for 500 years using a latitudinal dependent background diffusivity (0.01 cm^{2}s^{-1} at Equator, 0.3 cm^{2}s^{-1} at 30°N/S and 0.17 cm^{2}s^{-1} elsewhere, Jochum, 2009) with bottom-enhanced diffusivity calculated from Eq. 2. This is then compared to a similar 500 year long run where the background and tidal induced diffusivities are replaced by the IDEMIX module, referred to as IDE, forced with only the conversion of barotropic to baroclinic tides using the same forcing as CONT (Jayne and St. Laurent, 2001; St. Laurent et al., 2002; Jayne, 2009). Analysis is carried out for the years 450-499.

One extra sensitivity simulation, IEDDY, includes an additional energy source from mesoscale eddies as calculated from the simple dissipation form of Eden and Greatbatch (2008), where mesoscale eddy energy is converted to internal wave energy by

$$\epsilon_{eddy} = 0.1 L^2 \sigma^3, \tag{6}$$

with L being the minimum of the first baroclinic Rossby radius of deformation and the Rhines scale, and $\sigma = f\mathbf{u}_z/N$ is the Eady growth rate. This parameterization of eddy forcing adds energy to the internal waves everywhere in the ocean, in particular near eddying currents such as the ACC, western boundary currents and the Tropics (see e.g. figure 1d of Eden et al., 2009).

Eddy forcing of IDEMIX can be implemented in different ways (Eden et al., 2014). Here we choose the simplest form of local injection in Eq. 3.

This may not be the ideal implementation, but the reasoning behind the simulation is to see what effect adding more energy to the parameterization has, not how the choice of injection optimizes the simulations (here we refer the reader to Eden et al., 2014; Pollmann et al., 2017). The background for the sensitivity experiment comes from the fact that IDEMIX falls short of explaining observed dissipation rates without mesoscale eddy forcing (Pollmann et al., 2017). However, as CONT is only forced with tidal forcing, the main comparison experiment, IDE, is also forced with tides only. For an energetically consistent implementation the eddy forcing should be calculated from the used thickness diffusivity (in our simulations calculated according to Danabasoglu and Marshall, 2007). Other ways to implement other energy would be from estimates of lee wave energy fluxes (Nikurashin and Ferrari, 2011; Melet et al., 2014). Our implementation compares with the horizontal structure of such estimates. The choice of Eq. 6 is based on the simplicity from the fact that it is already directly implemented in POP2 (Eden and Greatbatch, 2008; Eden et al., 2009). IEDDY will be used only when discussing adding extra forcing to the IDEMIX parameterization. Note that the simple additional energy source by Eq. 6 is most likely an overestimation of the effect of eddies (as discussed in Eden et al., 2014).

In order to revisit the Indo-Pacific upwelling discussed by Jochum and Eden (2015), a set of three ocean/ice simulations with COREv2 Normal Year Forcing (Large and Yeager, 2004) with a sea surface salinity restoring timescale of one month are performed for both parameterizations of mixing. Each set consists of a 500 year control simulation, CONTF and IDEF. Each control simulation is accompanied by branched runs from year 300: One where winds over the Southern Ocean south of 35°S are shut off by multiplying the wind stress with a value $p = 0$, CONTF00 and IDEF00, and one where the Southern Ocean winds are increased by 50% by setting $p = 1.5$, CONTF15 and IDEF15. Between 35 and 25°S p is reduced linearly to 1. The wind profiles are depicted in Fig. 1. Each branch is run for 200 years. The forced simulation are analyzed for years 490-499. The model setups are summarized in table 1.

Reducing the background diffusivity in simulations using IDEMIX comes with the risk of making the model more prone to numerical noise, but this has been found only to pose issues in marginal seas (e.g. the Baltic and Caspian Seas, which only span few grid points and are not connected to the major basins in the coarse resolution POP2), for which reason the background diffusivities in these basins are set to the same value in IDEMIX simulations

as in the control simulations.

Section 3 first considers the coupled simulations and response in climate, and then deals with the two sets of forced simulations.

3. Results

3.1. Coupled simulations

We begin by assessing the differences between the two coupled simulations, CONT and IDE, beginning with the diffusivities followed by the differences in climatology. Global maps of the diffusivities (in this case only background diffusivities and tidal mixing as calculated by Eq. 2 in CONT and diffusivities as calculated by Eq. 3 and 5 in IDE) are presented in Fig. 2, averaged over three depth intervals: 0.2-1 km, 1-2 km and 2-4 km. The upper 200 m have been excluded because mixed and boundary layer diffusivities in IDE contaminate the signal of the thermocline structure due to the low stratifications within these. The pattern of bottom enhanced diffusivity due to topography is the same for the two simulations at all depths. This is expected as both parameterizations have the same tidal energy induced at the same bottom cells. The difference is in how the energy is distributed globally, as only 1/3 of the energy is dissipated locally in CONT and the rest is not considered but assumed to contribute to the background diffusivity, whereas IDE injects all the energy and distributes it through Eq. 3. CONT is largely characterized by the latitudinal dependent background diffusivity (Jochum, 2009), whereas IDE is characterized strongly by the bottom topography and displays a more heterogeneous diffusivity pattern. The diffusivities have been observed to be heterogeneous (Whalen et al., 2012; Pollmann et al., 2017), although the pattern here does lack much of the observed structure, likely due to only using tidal energy as forcing. In all depth intervals, IDE has large regions of reduced diffusivities compared to CONT. In the upper layer, the three major basins all have smaller diffusivities in IDE than CONT, showing a tendency for very small thermocline diffusivities. However, regions of larger diffusivities are also present, which is particularly connected to regions of weak stratification in the high latitudes and over rough topography. Between 1-2 km in the Equatorial band, the Pacific and the South Australia Basin have lower diffusivities than the imposed background level in CONT, which is also valid for the 2-4 km interval. These regions are associated with abyssal plains with very low tidal energy input to the internal waves. The diffusivities close to rough topography, on the other hand, are generally the

same magnitude or somewhere even larger in IDE. This suggests that more energy is dissipated locally (or at least very close to injection) in IDE than the 1/3 used in CONT, and that the horizontal propagation of E is very weak compared to the vertical propagation term and the dissipation.

The left panel of Fig. 3 shows the distribution of grid points with a specific diffusivity. It is evident that where CONT has a very narrow peak around diffusivities just above 10^{-5} m^{2}s^{-1}, IDE has a more broad distribution of diffusivities, but also has distinct peaks at the two cut-off ends of the spectrum. Note that there is almost an order magnitude more points at the higher end of the spectrum in IDE than CONT due to the global dependency on stratification throughout the water column and not just near the bottom, which increases the diffusivity greatly in the surface layers within the mixed layer. The histogram also displays that a large number of grid points in IDE have diffusivities smaller than in CONT. From Fig. 2 we can infer that these points are in particular located in the Tropics and Sub-Tropics over abyssal plains and are not only confined to the deep ocean but also the upper parts of the ocean below the mixed and boundary layers.

On the right panel of Fig. 3 globally averaged profiles of the diffusivities are plotted. Solid lines indicate diffusivities over rough topography (defined here as bathymetry slopes larger than 0.01), and dashed lines indicate diffusivities over smooth topography. Only water columns with depths greater than 500 m are included. This shows that CONT has up to an order magnitude larger diffusivities than IDE in the very deep ocean over smooth topography. This is a result of the deep ocean points which have very little injection of tidal energy in the abyssal plains, causing many points to be of small magnitude in IDE (see Fig. 2) in the deep ocean, in contrast to the rather large background diffusivity in CONT. Between 1-4 km depth, the two models have very similar global profiles. In the upper 200 m the stratification dependency in IDE shows up in very large diffusivities.

The global power consumption to raise the potential energy due to vertical mixing is estimated as the global integral

$$\mathcal{P} = \int_V \kappa \rho \frac{\partial b}{\partial z} dV, \tag{7}$$

where $b = g\delta\rho/\rho_0$ is buoyancy, which yields a total of 0.26 TW for CONT of which 0.12 TW is dissipated below 500 m, and 0.30 TW for IDE of which only 0.08 TW is dissipated below a depth of 500 m.

The vertical distribution of dissipated energy per unit volume divided by the density of water, yielding the dissipation per unit mass, is shown in Fig. 4 for CONT (black) and IDE (red) along with a global composite of fine-structure estimates (Kunze, 2017, magenta line). The dashed red curve is calculated directly from Eq. 4, whereas solid curves are calculated by dividing the integrand of Eq. 7 with the mixing efficiency. This estimate is derived as no direct estimate of dissipation is calculated in CONT. Unstably stratified grid points are omitted as assumptions for fine structure as well as parameterizations are not valid under these conditions. As can be seen, using diffusivity and stratification to derive the dissipation in IDE (solid red) underestimates the amount of dissipation calculated by Eq. 4 (dashed red). Both parameterizations show too much dissipation in the deep regions of the ocean and in particular at mid-depth, but dissipation in CONT is more in line with observations above 1 km, where the dissipation rate in IDE is too small and does not resemble fine-structure estimates. That both models have too much dissipation in the deep ocean suggests too much deep dissipation of tidal energy. For IDE, discrepancies with observations might be related to either a poor representation of propagation of energy or missing energy sources in the upper ocean. To investigate the latter, the sensitivity study IEDDY has been carried out, where conversion of mesoscale eddy energy to internal wave energy is added in Eq. 3. The resulting dissipation profile (from Eq. 4) is added in Fig. 4 as the dashed blue line. It is seen that eddy energy forcing increases the interior dissipation rates in particular in the upper 2 km. A different choice of implementation of mesoscale eddy dissipation may alter this distribution, but this is beyond the scope of this study. It should be noted that the fine-structure estimates sample mostly the major ocean basins whereas the model estimates are global averages. Furthermore, the uncertainty is large in the deep ocean where observations are sparse (Kunze, 2017).

The average AMOC strength at 26°N is 14.3 Sverdrups (1 Sv $= 10^6$ m^{3}s^{-1}) for CONT and 13.4 Sv for IDE. Thus, the different dissipation in IDE is accompanied by a weaker AMOC. This may be a reflection in changed mixing in waters associated with deep water formation (Melet et al., 2016), although the AMOC reduction is not necessarily a direct result of the mixing parameterization but could be due to feedbacks in buoyancy or wind forcing from the atmosphere. However, wintertime convection depths in the North Atlantic are shallower in IDE than CONT, suggesting the AMOC reduction to be caused by reduced production of North Atlantic Deep Water (not shown).

Changes in the surface fields are generally small. Fig. 5 shows the sea surface temperature (SST) difference between IDE and CONT. Note that CONT has several biases (discussed in Shields et al., 2012), the most prominent ones being related to the western boundary currents and the upwelling regions such as the Benguela system west of southern Africa, where the amplitude of the biases are larger in IDE than CONT. The root-mean-squared error (RMSE) for CONT is 1.67 and somewhat larger for IDE with a RMSE of 1.90 (reduced to 1.80 in IEDDY, not shown).

Superimposed on the upper panel of Fig. 5 is the 15% sea ice concentration lines for CONT (black) and IDE (red). The two lines almost coincide, with IDE having a slightly more northward extent of sea ice in the Southern Ocean, and a slightly more southward extent in the Bering Sea. The North Atlantic sea ice extent is comparable, but sea ice concentrations are greater within parts of the ocean in IDE, most remarkably in the Baffin Bay (not shown). The sea ice extent is already too large in CONT (Shields et al., 2012), but is stable within the two parameterization schemes.

The lower panel of Fig. 5 shows the precipitation difference between IDE and CONT. Differences are confined to the Tropics. Two major patterns are visible. The first is an increase in precipitation in the double-ITCZ seen over the Pacific and Atlantic. These changes are rather small and related to the modest increase in SST in the upwelling regions. The biggest change occurs over the Indian Ocean and the Indonesian seas, related to a difference in SST in the same region. This precipitation pattern is related to the diffusivity in the Banda Sea region (Jochum and Potemra, 2008). In CONT, this region has enhanced background vertical diffusivity made to match observations of a large tidally induced mixing in the region, which causes a reduction in the SST which heavily influences precipitation. This mixing is not captured in IDE, which may either be due to a too low energy input from tides or in the way the energy propagates into the region in the IDEMIX parameterization.

Fig. 6 shows the meridional distribution of temperature difference between the two simulations, overlaid with contours (5°C intervals) from CONT (dashed), IDE (solid) and World Ocean Atlas 2009 (WOA, Locarnini et al., 2010, dotted). A large difference in the simulations is in the thermocline. IDE has a sharper and shallower thermocline which causes temperatures to be cooler between 100 and 1000 m depth. This is seen in particular in the waters between 5 and 15 °C which are shallower in IDE compared to both CONT and observations, causing the temperature stratification to be in less agreement with observations. At mid-depth, however, IDE is closer to ob-

servations seen in the close agreement with the observed 5°C isotherm. The rest of the global ocean has temperature differences with amplitude less than 0.5°C. The large differences between CONT and IDE occur in the upper km which is also the region of the largest discrepancy in dissipated energy in Fig. 4, and in the region of small diffusivities in the Pacific and Atlantic, causing a reduced diffusion of heat from the surface, making the deep ocean largely colder and lifting the isotherms relatively to CONT. Evidently, the amount of energy used for mixing, but also its distribution vertically and horizontally, plays a major role in setting the thermocline structure (in agreement with earlier studies such as Bryan, 1987; Samelson, 1998; Melet et al., 2016).

3.2. Forced experiments

We now turn to the forced simulations with changed wind stress. Resulting diffusivities, SSTs and thermocline structure are similar as for the coupled simulations (not shown) and will not be discussed further, as the focus of the forcing experiments is how the ocean responds to changes in forcing.

As can be seen in Fig. 1, the wind stress for $p = 1.5$ peaks at almost 0.2 $\mathrm{N/m^2}$ compared to 0.13 for $p = 1.0$. This change in wind stress alters the wind stress curl over the Southern Ocean and forces increased Ekman driven upwelling. For $p = 0$, the wind stress curl is zero and the corresponding Ekman driven upwelling is zero.

The residual meridional overturning circulations (RMOC, from hereon simply MOC), defined as the sum of the Eulerian mean and the eddy-induced overturning streamfunctions for the Atlantic (AMOC) and Indo-Pacific (PMOC, calculated as the global MOC subtracted the AMOC, minimum overturning north of 35S) averaged over the last 10 model years are listed in Table 4. The AMOC strength at 26°N is plotted in Fig. 7. CONTF has an AMOC strength of 15.7 Sv after 300 years and 15.8 Sv after 500 years compared to 13.5 Sv at both times in IDEF, suggesting that although not nearly equilibrated, the model is stable enough for our purposes. Also, the weaker AMOC seen in the coupled runs is also reflected in the forced runs. As with coupled runs, shallow North Atlantic boundary layer depths in IDE suggest a reduced production of North Atlantic Deep Water to be the cause of this.

As can be seen, increasing (decreasing) winds results in an initial, quick response where the AMOC increases (decreases) over the first 30 years. After this initial, transient response, a more gradual increase (decrease) follows.

The initial relative increase in AMOC strength in CONTF15 is 9% after 30 years of perturbation and by the end in year 500 the AMOC strength has increased by 18%. For IDEF15 relative to IDEF the values are 12% and 24%, respectively. Correspondingly for $p = 0.0$ the values of CONTF00 relative to CONTF are a 16% and 26% decrease in AMOC strength, and for IDEF00 the decrease corresponds to 18% and 31% relative to IDEF. It follows that the relative sensitivity towards changing wind stress is larger in simulations with the Olbers and Eden (2013) parameterization, whereas the absolute values are comparable.

The PMOC for the six experiments is plotted in Fig. 8 along with the average depth of the $\sigma_\theta = 27.7$ kg m^{-3} isopycnal. The relative increase in strength of the upwelling (PMOC in Table 4) for IDEF00 is 194%, and the relative reduction in IDEF15 is 17%. For CONTF00 and CONTF15 these numbers are 106% and 27%, respectively. The absolute changes in PMOC in experiments with $p = 0$ compares roughly to the strength of the AMOC in the corresponding runs.

Thus, as in Jochum and Eden (2015), simulations without any wind stress over the Southern Ocean yield an enhanced upwelling in the Indo-Pacific, which at least in part compensates the missing upwelling in the Southern Ocean and sustains an AMOC at least for several centuries following the beginning of the wind stress perturbation.

The 27.7 kg m^{-3} isopycnal shoals 200-300 m in the Pacific and deepens in the Southern Ocean in both experiments with $p = 0$, compared to simulations with $p = 1$, flattening and shallowing the isopycnal. For $p = 1.5$ the isopycnal steepens over the Southern Ocean and deepens by up to 200 m at 40°S and about 100 m north of this latitude. Thus, while the relative changes in streamfunction are different with the two parameterizations, the impact of the winds on the pycnocline depth is very similar in the two cases. Thus, despite diffusivities depending on the stratification, the Indo-Pacific overturning response in IDEF simulations is, in absolute sense, comparable to the response in CONTF simulations.

4. Summary and discussion

Three coupled ocean, atmosphere and sea ice (including a sensitivity run) and six forced ocean/sea ice simulations, have been carried out to assess the impact of the vertical mixing parameterization IDEMIX (Olbers and Eden, 2013) in the ocean component of CCSM4. The coupled simulations, CONT,

IDE and the sensitivity study IEDDY, are run for 500 years and the forced CONTF and IDEF are run for 300 years, at which time wind stress perturbations over the Southern Ocean are performed and simulations are run for 200 years more. It has been shown that the way in which the dissipation of energy is localized globally impacts the ocean state and related climate (in agreement with earlier studies such as Samelson, 1998; Melet et al., 2013). The most prominent differences occur in setting the thermocline depth. Reduced thermocline diffusivities cause less heat to be mixed downward, causing a sharper and shallower thermocline, consistent with other studies (Melet et al., 2016). The relationship between thermocline structure and diffusivities implies that large differences in heat and carbon storage can occur over long timescales depending on the mixing parameterization, something that is left for future studies to assess.

For the coupled simulations minor changes are observed in the SSTs and precipitation fields. The representation of precipitation and SSTs in IDE is worse than in CONT. However, compared to the already existing biases in CONT, the differences between IDE and CONT are small. Also, the overall climate state is very comparable in the two runs. The SST differences in IDE are adding to already existing biases, which implies that with improved parameterizations of vertical mixing the biases might be reduced.

The Benguela upwelling system is one area in the model with an already existing bias that gets worse in IDE. The nature of the bias has been studied and is thought to be a result of several processes (Xu et al., 2014; Harlaß et al., 2015). In particular, vertical mixing has been suggested to be one of the contributing mechanisms in generating temperature biases in POP2 (Xu et al., 2014). Our results support this hypothesis and suggest that either energy forcing or propagation is not adequately represented in the region. It is also possible that a more realistic description of vertical mixing enhances the SST bias because a previous compensation with other model errors is relaxed. The same holds for other model biases, highlighting the need for more careful representation of vertical mixing in climate models.

While the errors in surface fields are larger in IDE than CONT in some areas, IDEMIX is developed from physical principles, whereas the existing parameterization uses the background mixing to match diffusivities to observations, which may not hold in studies of paleoclimate or future predictions. It is furthermore interesting to note that while both simulations are missing energy sources from e.g. mesoscale eddies, the contribution from these is easily implemented as forcing terms in IDEMIX if one can calculate the en-

ergy transfer to the internal wave field, whereas the existing model requires a new parameterization for each energy source that needs to be included. Using IDEMIX, the problem is reduced to the investigation of how and where energy enters the internal wave field (Eden et al., 2014).

The large amount of grid points with diffusivities below 10^{-6} m^2 s^{-1} in IDE seen in Fig. 2 and in the left panel of Fig. 3 may not be realistic, but suggest that more energy forcing to the internal wave field is needed. Our sensitivity study, IEDDY, is preliminary, but indicates that adding energy sources in IDEMIX might indeed bring the simulation closer to observed estimates of dissipation rates in the thermocline and thus improve climate simulations. However, this requires careful treatment of each individual source of internal wave energy. For instance, for coarse resolution ocean models, tidal energy may be put in too deep in the water column which might in turn affect overturning strengths (Schmittner and Egbert, 2014). Other improvements might be found by separate treatment of low mode internal waves (Eden and Olbers, 2014).

Finally, the present results show that trapped waves and their dissipation in the Banda Sea is not well represented in the current parameterization of IDEMIX. It is not clear how such waves, which are unresolved in climate models, and their associated dissipation should be parameterized and implemented in IDEMIX, but as with the case of the Banda Sea, these are of climatic importance and other areas might exist where similar wave dissipation is important in setting the mixing strength.

With regards to the forced simulations, we find that the relative importance of the Southern Ocean wind stress on AMOC strength is larger in IDEF than CONTF, whereas absolute changes are similar. It is therefore likely that the difference in relative importance of winds is a result of the changed background state and its associated weaker AMOC observed in IDEF. Both parameterizations find a similar compensation in the Indo-Pacific when the wind stress is shut off over the Southern Ocean, in agreement with Jochum and Eden (2015). A key difference compared to their results is that without wind stress the AMOC is declining toward a weak state, whereas they found the AMOC to be independent of the wind stress. However, the nature of forced ocean/ice experiments do not allow for atmospheric feedbacks which might modify this result (Rahmstorf and England, 1997).

Acknowledgements

This study was supported by The Danish Council for Independent Research, Natural Sciences, 4002-00397. Simulations were done with support from the High Performance Computing Centre at the University of Copenhagen. The authors would also like to thank Eric Kunze for fine structure estimates of internal wave dissipation and Nils Brüggemann and Dirk Olbers for helpful comments.

References

Bryan, F., 1987. Parameter sensitivity of primitive equation ocean general circulation models. J. Phys. Oceanogr. 17, 970–985. doi:10.1175/1520-0485(1987)017<0970:PSOPEO>2.0.CO;2.

Bryan, K., Lewis, L., 1979. A water mass model of the world ocean. J. Geophys. Res. 84, 2503–2517. doi:10.1029/JC084iC05p02503.

Danabasoglu, G., Bates, S., Briegleb, B., Jayne, S., Jochum, M., Large, W., Peacock, S., Yeager, S., 2012. The ccsm4 ocean component. J. Climate 25, 1361–1389. doi:10.1175/JCLI-D-00091.1.

Danabasoglu, G., Marshall, J., 2007. Effects of vertical variations of thickness diffusivity in an ocean general circulation model. Ocean Modell. 18, 122–141.

Eden, C., Czeschel, L., Olbers, D., 2014. Toward energetically consistent ocean models. J. Phys. Oceanogr. 44, 3160–3184. doi:10.1175/JPO-D-13-0260.1.

Eden, C., Greatbatch, R., 2008. Towards a mesoscale eddy closure. Ocean Modell. 20, 223–239. doi:10.1016/j.ocemod.2007.09.002.

Eden, C., Jochum, M., Danabasoglu, G., 2009. Effects of different closures for thickness diffusivity. Ocean Modell. 26, 47–59.

Eden, C., Olbers, D., 2014. An energy compartment model for propagation, nonlinear interaction, and dissipation of internal gravity waves. J. Phys. Oceanogr. 44, 2093–2106. doi:10.1175/JPO-D-13-0224.1.

Egbert, G., Ray, R., 2000. Significant dissipation of tidal energy in the deep ocean inferred from satellite altimeter data. Nature 405, 775–778. doi:10.1038/35015531.

Gent, P.R., Danabasoglu, G., Donner, L.J., Holland, M.M., Hunke, E.C., Jayne, S.R., Lawrence, D.M., Neale, R.B., Rasch, P.J., Vertenstein, M., Worley, P.H., Yang, Z.L., Zhang, M., 2011. The community climate system model version 4. J. Climate 24, 4973–4991. doi:10.1175/2011JCLI4083.1.

Gent, P.R., Large, W.G., Bryan, F.O., 2001. What sets the mean transport through drake passage. J. Geophys. Res. 106, 2693–2712. doi:10.1029/2000JC900036.

Harlaß, J., Latif, M., Park, W., 2015. Improving climate model simulation of tropical atlantic sea surface temperature: The importance of enhanced vertical atmospher model resolution. Geophys. Res. Lett. 42, 2401–2408. doi:10.1002/2015GL063310.

Harrison, M., Hallberg, R., 2008. Pacific subtropical cell response to reduced equatorial dissipation. J. Phys. Oceanogr. 38, 1894–1912. doi:10.1175/2008JPO3708.1.

Heyney, F., Wright, J., Flatté, S., 1986. Energy and action flow through the internal wave field: An eikonal approach. J. Geophys. Res. 91 (C7), 8487–8495. doi:10.1029/JC091iC07p08487.

Jayne, S., 2009. The impact of abyssal mixing parameterizations in an ocean general circulation model. J. Phys. Oceanogr. 39, 1756–1775. doi:10.1175/2009JPO4085.1.

Jayne, S., St. Laurent, L., 2001. Parameterizing tidal dissipation over rough topography. Geophys. Res. Let. 28 (5), 811–814. doi:10.1029/2000GL012044.

Jochum, M., 2009. Impact of latitudinal variations in vertical diffusivity on climate simulations. J. Geophys. Res. 114, C01010. doi:10.1029/2008JC005030.

Jochum, M., Briegleb, B., Danabasoglu, G., Large, W., Norton, N., Jayne, S., Alford, M., Bryan, F., 2013. The impact of oceanic near-inertial waves on climate. J. Climate 26, 2833–2844. doi:10.1175/JCLI-D-12-00181.1.

Jochum, M., Eden, C., 2015. The connection between southern ocean winds, the atlantic meridional overtuning circulation, and indo-pacific upwelling. J. Climate 28, 9250–9257. doi:10.1175/JCLI-D-15-0263.1.

Jochum, M., Potemra, J., 2008. Sensitivity of tropical rainfall to banda sea diffusivity in the community climate system model. J. Climate 21, 6445–6454. doi:10.1175/2008JCLI2230.1.

Kuhlbrodt, T., Griesel, A., Montoya, M., Levermann, A., Hofmann, M., Rahmstorf, S., 2007. On the driving processes of the atlantic meridional overturning circulation. Rev. Geophys. 45, RG2001. doi:10.1029/2004RG000166.

Kunze, E., 2017. Internal-wave-driven mixing: Global geography and budgets. Journal of Physical Oceanography 47, 1325–1345. doi:10.1175/JPO-D-16-0141.1.

Large, W., Yeager, S., 2004. Diurnal to decadal global forcing for ocean and sea-ice models: the data sets and flux climatologies. NCAR.

Ledwell, J., Watson, A., Law, C., 1998. Mixing of a tracer in the pycnocline. Journ. Geophys. Res. 103, 21499–21529. doi:10.1029/98JC01738.

Locarnini, R., Mishonov, A., Antonov, J., Boyer, T., Garcia, H., Baranova, O., Zweng, M., Johnson, D., 2010. World Ocean Atlas 2009, Volume 1: Temperature. NOAA Atlas NESDIS 68.

MacKinnon, J.A., et al., 2017. Climate process team on internal-wave driven ocean mixing. Bull. Am. Meteorol. Soc. In Press. doi:10.1175/BAMS-D-16-0030.1.

Marotzke, J., 1997. Boundary mixing and the dynamics of three-dimensional thermohaline circulation. J. Phys. Oceanography 27, 1713–1728. doi:10.1175/1520-0485(1997)027<1713:BMATDO>2.0.CO;2.

McComas, C., Müller, P., 1981. Time scales of resonant interactions among oceanic internal waves. J. Phys. Oceanogr. 11, 139–147. doi:10.1175/1520-0485(1981)011<0139:TSORIA>2.0.CO;2.

Melet, A., Hallberg, R., Legg, S., Nikurashin, M., 2014. Sensitivity of the ocean state to lee wave-driven mixing. J. Phys. Oceanogr. 44, 900–921. doi:10.1175/JPO-D-13-072.1.

Melet, A., Hallberg, R., Legg, S., Polzin, K., 2013. Sensitivity of the ocean state to the vertical distribution of internal-tide-driven mixing. J. Phys. Oceanogr. 43, 602–615. doi:10.1175/JPO-D-12-055.1.

Melet, A., Legg, S., Hallberg, R., 2016. Climate impacts of parameterized local and remote tidal mixing. J. Climate 29, 3473–3500. doi:10.1175/JCLI-D-15-0153.1.

Munday, D., Johnson, H., Marshall, D., 2013. Eddy saturation of equilibrated circumpolar currents. J. Phys. Oceanogr. 43, 507–532. doi:10.1175/JPO-D-12-095.1.

Munk, W., 1966. Abyssal recipes. Deep Sea Res. 13, 707–730. doi:10.1016/0011-7471(66)90602-4.

Munk, W., Wunsch, C., 1998. Abyssal recipes ii: energetics of tidal and wind mixing. Deep Sea Res. 45, 1977–2010. doi:10.1016/S0967-0637(98)00070-3.

Nikurashin, M., Ferrari, R., 2010. Radiation and dissipation of internal waves generated by geostrophic motions impinging on small-scale topography: Theory. J. Phys. Oceanogr. 40, 1055–1074. doi:10.1175/2009JPO4199.1.

Nikurashin, M., Ferrari, R., 2011. Global energy conversion rate from geostrophic flows into internal lee waves in the deep ocean. Geophys. Res. Letters 38, L08610. doi:10.1029/2011GL046576.

Nycander, J., 2005. Generation of internal waves in the deep ocean by tides. J. Geophys. Res. 110, C10028. doi:10.1029/2004JC002487.

Olbers, D., Eden, C., 2013. A global model for the diapycnal diffusivity induced by internal gravity waves. J. Phys. Oceanogr. 43, 1759–1779. doi:10.1175/JPO-D-12-0207.1.

Osborn, T., 1980. Estimates of the local rate of vertical diffusion from dissipation measurements. J. Phys. Oceanogr. 10, 83–89. doi:10.1175/1520-0485(1980)010<0083:EOTLRO>2.0.CO;2.

Pollmann, F., Eden, C., Olbers, D., 2017. Evaluating the global internal wave model idemix using finestructure methods. J. Phys. Oceanogr. 47, 2267–2289.

692 Polzin, K., Toole, J., Ledwell, J., Schmitt, R., 1997. Spatial variability of
693 turbulent mixing in the abyssal ocean. Science 276, 93+96. doi:10.1126/
694 science.276.5309.93.

695 Rahmstorf, S., England, M., 1997. Influence of southern hemisphere winds
696 on north atlantic deep water flow. J. Phys. Oceanogr. 27, 2040–2054.
697 doi:10.1175/1520-0485(1997)027<2040:IOSHWO>2.0.CO;2.

698 Samelson, R., 1998. Large-scale circulation with locally enhanced vertical
699 mixing. J. Phys. Oceanogr. 28, 712–726. doi:10.1175/1520-0485(1998)
700 028<0712:LSCWLE>2.0.CO;2.

701 Sandström, J., 1908. Dynamische verusche mit meerwasser. Annals in Hy-
702 drodynamic Marine Meteorology 1, 6–23.

703 Schmittner, A., Egbert, G., 2014. An improved parameterization of tidal
704 mixing. Geosci. Model Dev. 7, 211–224. doi:10.5194/gmd-7-211-2014.

705 Shields, C., Bailey, D., Danabasoglu, G., Jochum, M., Kiehl, J., Levis, S.,
706 Park, S., 2012. The low-resolution ccsm4. J. Climate 25, 3993–4014.
707 doi:10.1175/JCLI-D-11-00260.1.

708 Simmons, H., Jayne, S., St. Laurent, L., Weaver, A., 2004. Tidally driven
709 mixing in a numerical model of the ocean general circulation. Ocean Mod-
710 ell. 6, 245–263. doi:10.1016/S1463-5003(03)00011-8.

711 St. Laurent, L., Simmons, H., Jayne, S., 2002. Estimating tidally driven
712 mixing in the deep ocean. Geophys. Res. Letters 29(23), 2106. doi:10.
713 1029/2002GL015633.

714 Toggweiler, J., Samuels, B., 1995. Effects of drake passage on the global
715 thermohaline circulation. Deep-Sea Res. 42, 477–500. doi:10.1016/
716 0967-0637(95)00012-U.

717 Toggweiler, J., Samuels, B., 1998. On the ocean's large-scale circulation
718 near the limit of no vertical mixing. J. Phys. Oceanogr. 28, 1832–1852.
719 doi:10.1175/1520-0485(1998)028<1832:OTOSLS>2.0.CO;2.

720 Waterhouse, A.F., et al., 2014. Global patterns of diapycnal mixing from
721 measurements of the turbulent dissipation rate. J. Phys. Oceanogr. 44,
722 1854–1872. doi:10.1175/JPO-D-13-0104.1.

723 Whalen, C., Talley, L., MacKinnon, J., 2012. Spatial and temporal variability
724 of global ocean mixing inferred from argo profiles. Geophys. Res. Let. 39,
725 L18612. doi:10.1029/2012GL053196.

726 Xu, Z., Chang, P., Richter, I., Kim, W., Tang, G., 2014. Diagnosing southeast
727 tropical atlantic sst and ocean circulation biases in the cmip5 ensemble.
728 Clim Dyn 43, 3123–3145. doi:10.1007/s00382-014-2247-9.

Tables

Table 1: Summary of model setups. Case explanation: OCN: ocean/sea ice. FULL: fully coupled. p is the SO wind multiplication factor

	Case	Mixing	p
CONT	FULL	St. Laurent et al. (2002)	–
IDE	FULL	Olbers and Eden (2013)	–
IEDDY	FULL	Olbers and Eden (2013); Eden and Greatbatch (2008)	–
CONTF00	OCN	St. Laurent et al. (2002)	0.0
CONTF	OCN	St. Laurent et al. (2002)	1.0
CONTF15	OCN	St. Laurent et al. (2002)	1.5
IDEF00	OCN	Olbers and Eden (2013)	0.0
IDEF	OCN	Olbers and Eden (2013)	1.0
IDEF15	OCN	Olbers and Eden (2013)	1.5

Table 2: Absolute strength in overturning circulations in the forced simulations. All units in Sv (1 Sv = 10^6 m^3 s^{-1}).

	AMOC	PMOC
CONTF00	11.7	-21.4
CONTF	15.8	-10.3
CONTF15	18.5	-7.5
IDEF00	9.5	-14.8
IDEF	13.5	-5.0
IDEF15	16.6	-4.1

Figures

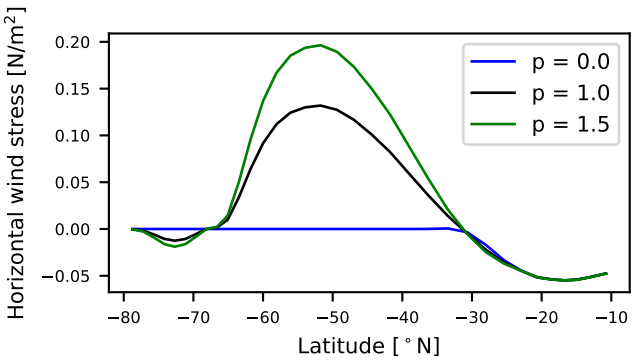

Figure 1: The horizontal wind stress over the Southern Ocean in the three experiments of each set of forced simulations.

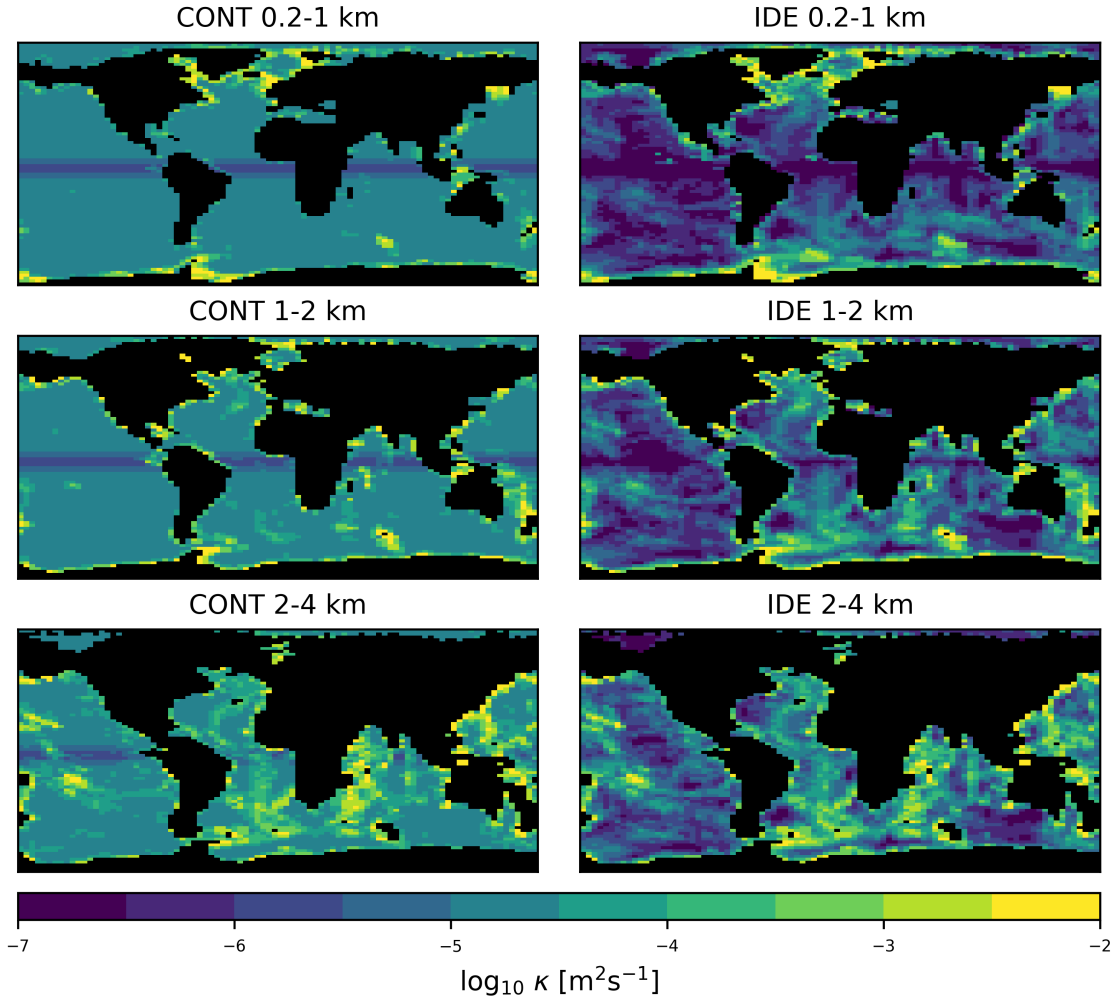

Figure 2: Global map of diffusivities for CONT (left column) and IDE (right column) averaged over 0.2-1 km depth (upper row), 1-2 km depth (middle row) and 2-4 km depth (bottom row).

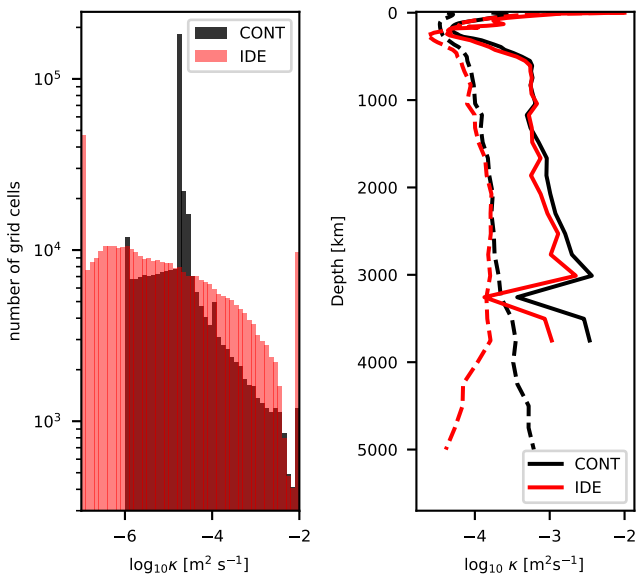

Figure 3: Left: Histogram of diffusivities in CONT (black) and IDE (pink). Red indicates the overlap of the two. Note the logarithmic vertical axis. Right: Globally averaged vertical diffusivity profile for CONT (black) and IDE (red). Solid lines indicate diffusivities over rough topography (slopes larger than 0.01) and dashed indicate smooth topography.

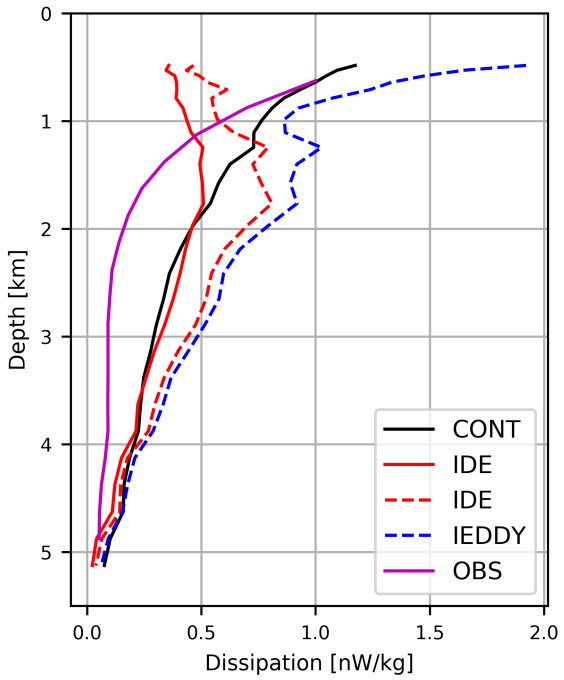

Figure 4: Globally integrated dissipation of energy for CONT (solid black), IDE (solid red) and observations (Kunze, 2017, solid magenta). The red dashed curve represents IDE evaluated using Eq. 4. The dashed blue line represents IEDDY where extra energy forcing is added to Eq. 3, evaluated using Eq. 4.

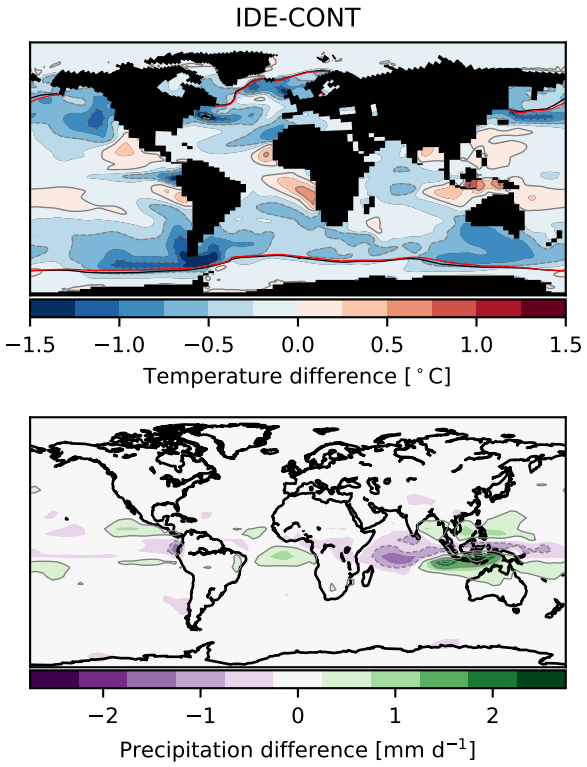

Figure 5: SST (upper) and precipitation (lower) difference between IDE and CONT.

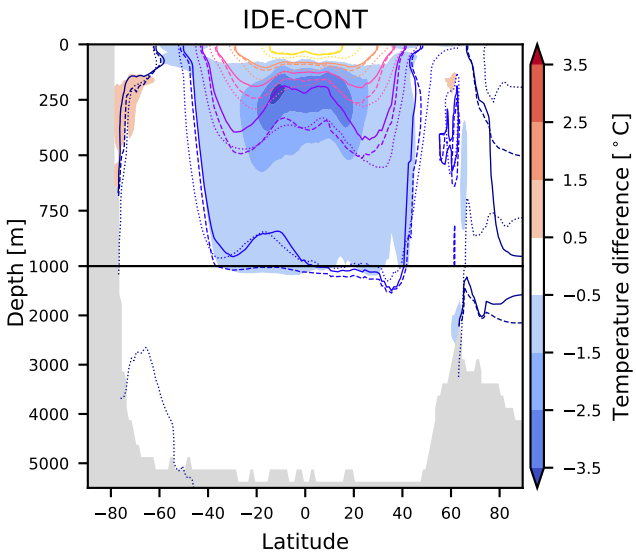

Figure 6: Difference between zonally averaged temperature in IDE and CONT. Overlying contours are zonally averaged potential temperature of CONT (dashed), IDE (full) and WOA (dotted). Contour interval is 5°C, ranging from 0°C (dark blue in polar regions) to 25°C (yellow). Note the non-linear vertical axis at 1000 m.

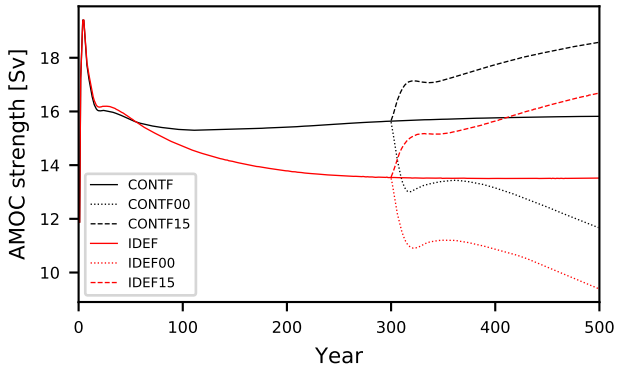

Figure 7: AMOC strength (in Sv) at 26°N in the forced simulations. Wind stress perturbations start at year 300.

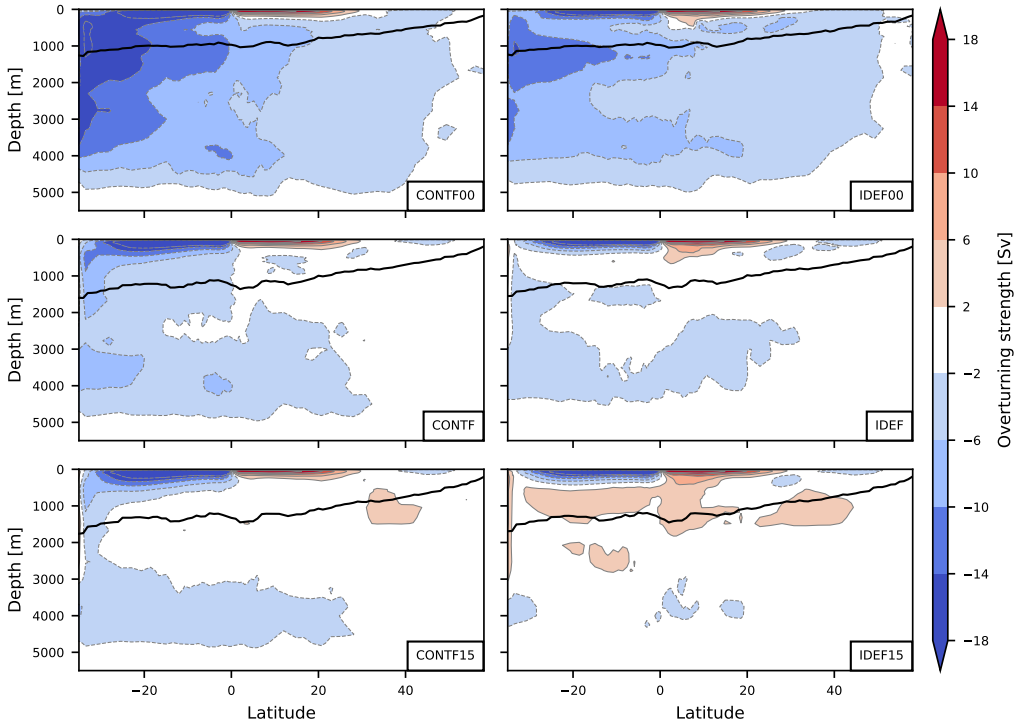

Figure 8: Indo-Pacific overturning stream function for the six forced experiments. Contour interval is 4 Sv. The black line denotes the average depth of the $\sigma = 27.7$ isopycnal.